SUPPORTING INFORMATION

Super-Compressible Coaxial Carbon Nanotube@Graphene Arrays with Invariant Viscoelasticity over −100 to 500 °C in Ambient Air

Lin Jing,[1, 2, ¶] Hongling Li,[3, ¶] Jinjun Lin,[3] Roland Yingjie Tay,[3] Siu Hon Tsang,[4] Edwin Hang Tong Teo[1, 3*] and Alfred Iing Yoong Tok[1, 2*]

[1] School of Materials Science and Engineering, Nanyang Technological University, 50 Nanyang Avenue, Singapore 639798, Singapore

[2] Institute for Sports Research, Nanyang Technological University, 50 Nanyang Avenue, Singapore 639798, Singapore

[3] School of Electrical and Electronic Engineering, Nanyang Technological University, 50 Nanyang Avenue, Singapore 639798, Singapore

[4] Temasek Laboratories@NTU, 50 Nanyang Avenue, Singapore 639798, Singapore

¶ These two authors contribute equally to this work.

* *Co-corresponding authors*. E-mail address: (E. H. T. T.) HTTEO@ntu.edu.sg; (A. I. Y. T.) MIYTOK@ntu.edu.sg.

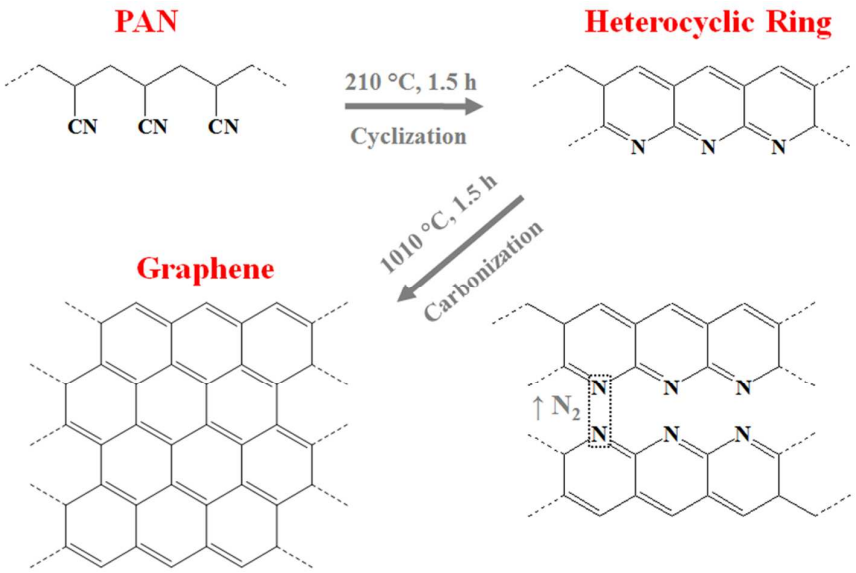

Scheme S1 Schematic illustration of the synthesis of graphene layers by means of two-step pyrolysis processes.[1]

Synthesis of CNT@Gr arrays. Typically, the PAN coated CNT arrays were first heated up to 210 °C and kept at this temperature for 1.5 h in Ar atmosphere, during which the PAN layers can be converted into condensed heterocyclic ring structure (cyclization).[1,2] Then the resulting samples were further pyrolyzed at 1010 °C for 1.5 h to transform the heterocyclic ring structure into planar graphene layers by splitting off the heterocyclic nitrogen (carbonization).[1,2] Finally, the conformal graphene layers can be successfully introduced onto the CNTs to form the coaxial CNT@Gr arrays.

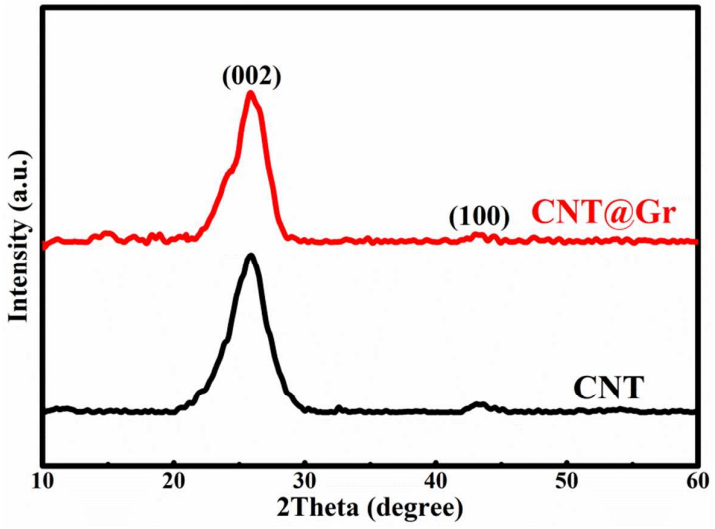

Figure S1 XRD profiles of CNT and CNT@Gr. The characteristic (002) and (100) diffraction peaks indicate that the crystallinity is well preserved for the CNT@Gr.

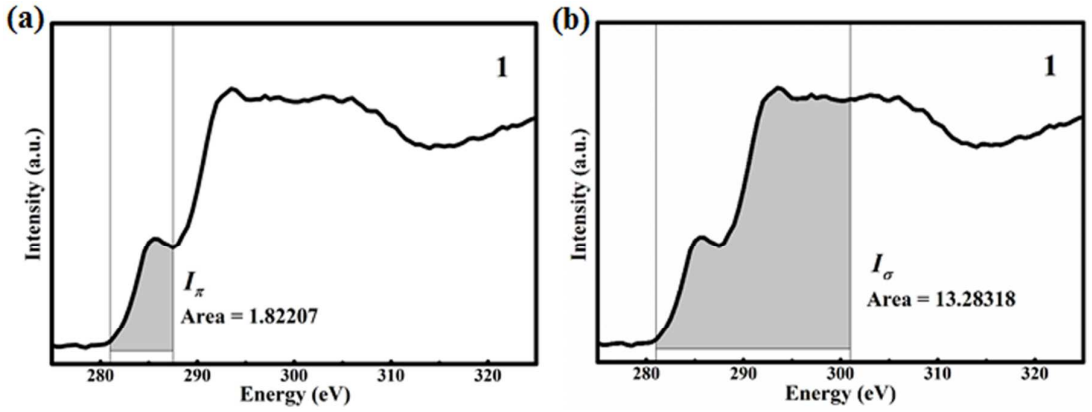

Figure S2 1s to π^* (I_π, shadow area in (a)) and total (I_σ, shadow area in (b)) peak intensities at the C K-edge for point 1.

Calculation of sp^2 / sp^3 ratio. Take the EELS spectrum of point 1 as an example, the 1s to π^* peak intensity at the C K-edge (background was subtracted prior acquiring the spectrum) was measured using an energy window of 5 eV (I_π, as shown in Figure S2a).[3] The total C K-edge intensity was then measured in a window of up to 20 eV extending from the edge onset and covering the π^* peak and majority of the 1s to σ^* peak (I_σ, as shown in Figure S2b).[3] Next, the sp^2 fraction x was calculated out according to $3x / (4 - x) = (I_\pi / I_\sigma) / (I_\pi^R / I_\sigma^R)$,[3,4] where I_π^R and I_σ^R are the 1s to π^* and total peak intensities of the 100% sp^2 carbon reference material, respectively. As a result, the sp^2 fractions for **points 1, 2 and 3** were extracted to be 0.75, 0.76 and 0.73, corresponding to **sp^2 / sp^3 ratios of 3, 3.17 and 2.70**, respectively.[5]

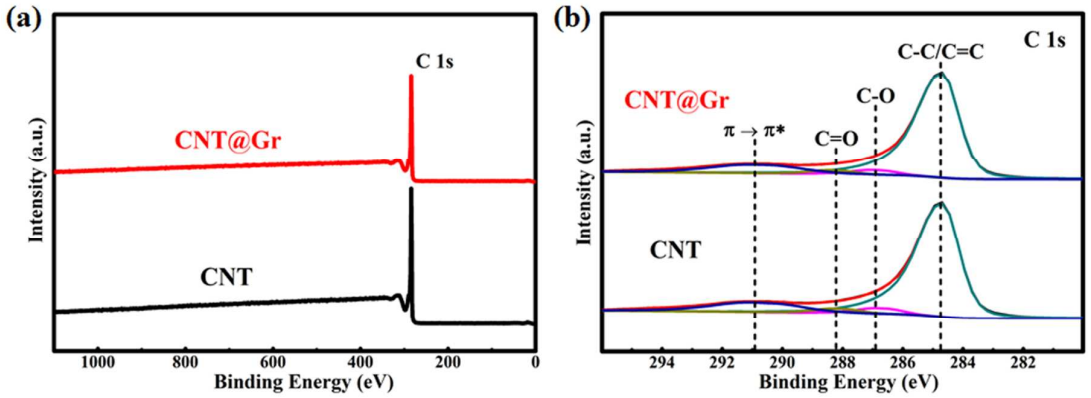

Figure S3 XPS survey and high resolution C 1s spectra of CNT and CNT@Gr, respectively.

XPS Analysis. XPS survey spectra show that no other elements except carbon (graphitic C 1s peak at 284.68 eV)[6] can be detected for both the CNT and CNT@Gr. Meanwhile, high resolution C 1s spectrum of the CNT@Gr displays no noticeable shift or change in the peaks assigned to sp^2 and sp^3 hybridized states as compared to those of the initial CNT.[7]

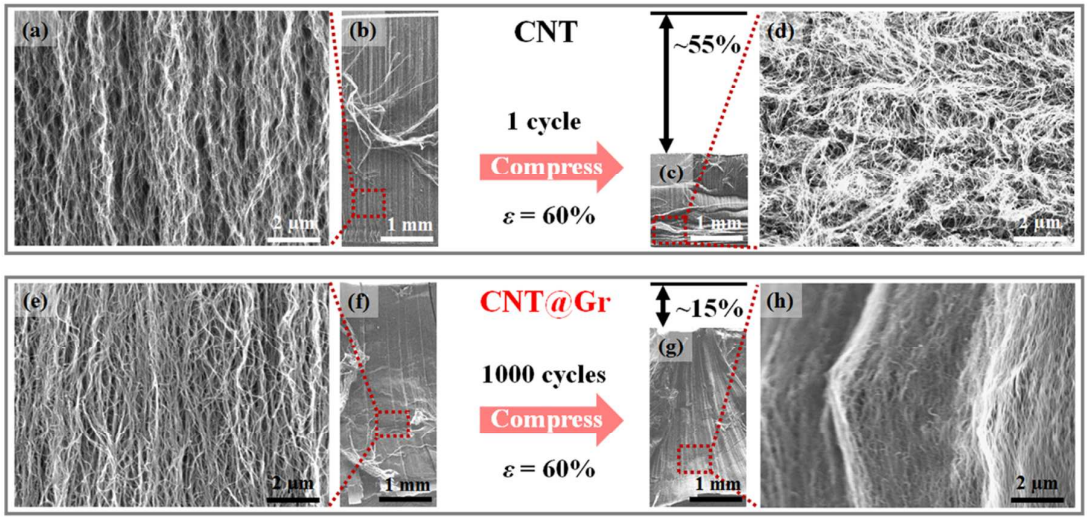

Figure S4 Cross-sectional SEM images of CNT (a−d) and CNT@Gr (e−h) arrays before and after 1 and 1000 compression cycles at strain (ε) = 60%, respectively. (a, d, e, h) are the zoom-in views of (b, c, f, g), respectively.

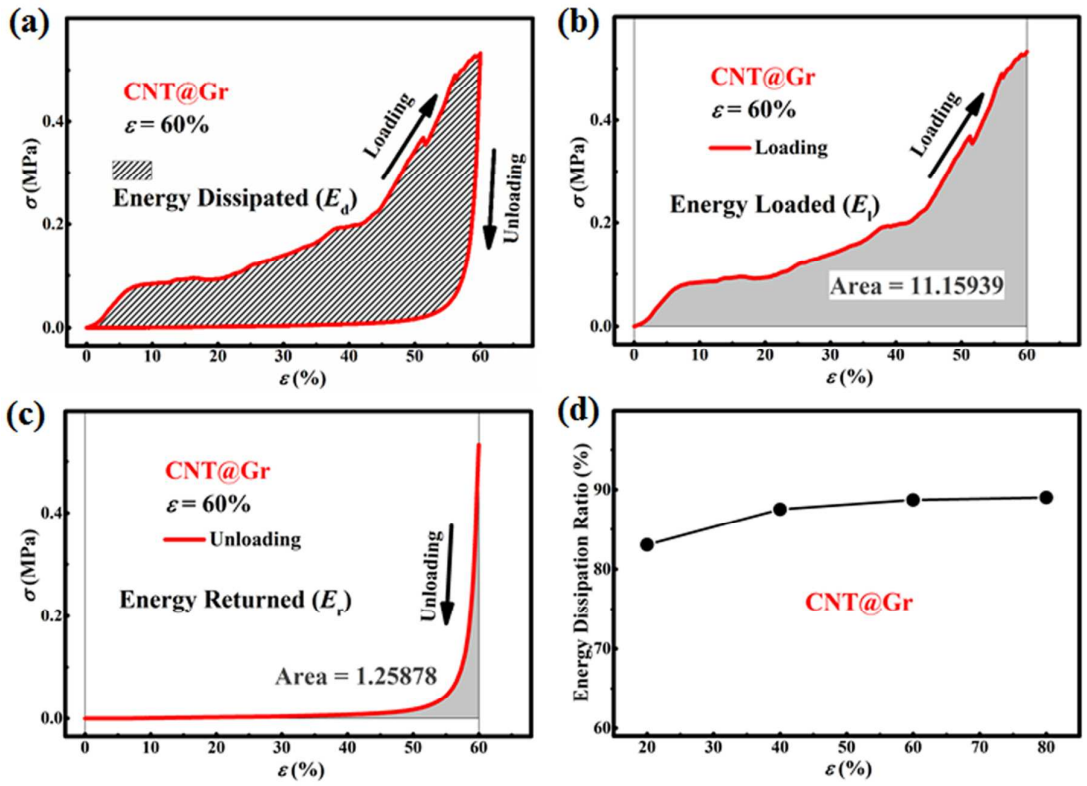

Figure S5 Energy dissipated (E_d, shadow area in (a)), energy loaded (E_l, shadow area in (b)) and energy returned (E_r, shadow area in (c)) for the first compression cycle at ε = 60%. (d) Energy dissipation ratios of CNT@Gr arrays at various applied ε.

Calculation of energy dissipation ratio. Take the first compression cycle at ε = 60% for the CNT@Gr arrays as an example, the energy dissipation ratio (E_d / E_l) is extracted from the corresponding stress (σ) *vs.* ε curves,[8] where E_d is the energy dissipated during the loading-unloading cycle (*i.e.* the area of the hysteresis loop, Figure S4a), E_l is the energy loaded during the compression loading process (*i.e.* the area under the loading σ *vs.* ε curve, which is integrated to be 11.15939, Figure S4b). Meanwhile, $E_d = E_l - E_r$, where E_r is the energy returned (*i.e.* the area under the unloading σ *vs.* ε curve, which is integrated to be 1.25878, Figure S4c). As a result, the energy dissipation ratio of the CNT@Gr arrays for the first compression cycle at ε = 60% could be calculated to be $E_d / E_l = (E_l - E_r) / E_l$ = (11.15939 - 1.25878) / 11.15939 ≈ 88.72%.

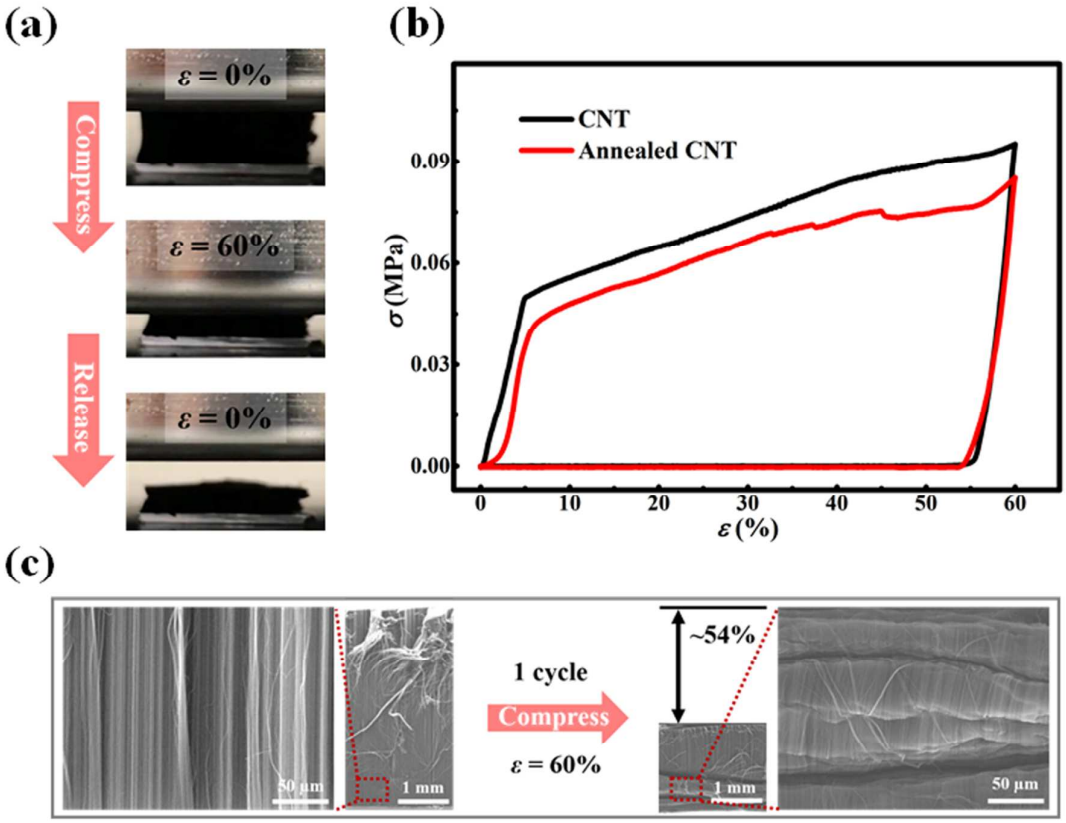

Figure S6 Compressive mechanical responses of annealed CNT arrays. (a) Annealed CNT arrays deform almost plastically upon uniaxial compression at ε = 60%. (b) Compressive stress σ *vs.* ε curves at ε = 60% of CNT arrays before and after high temperature annealing. (c) Cross-sectional SEM images of the annealed CNT arrays before and after 1 cycle of compression at ε = 60%.

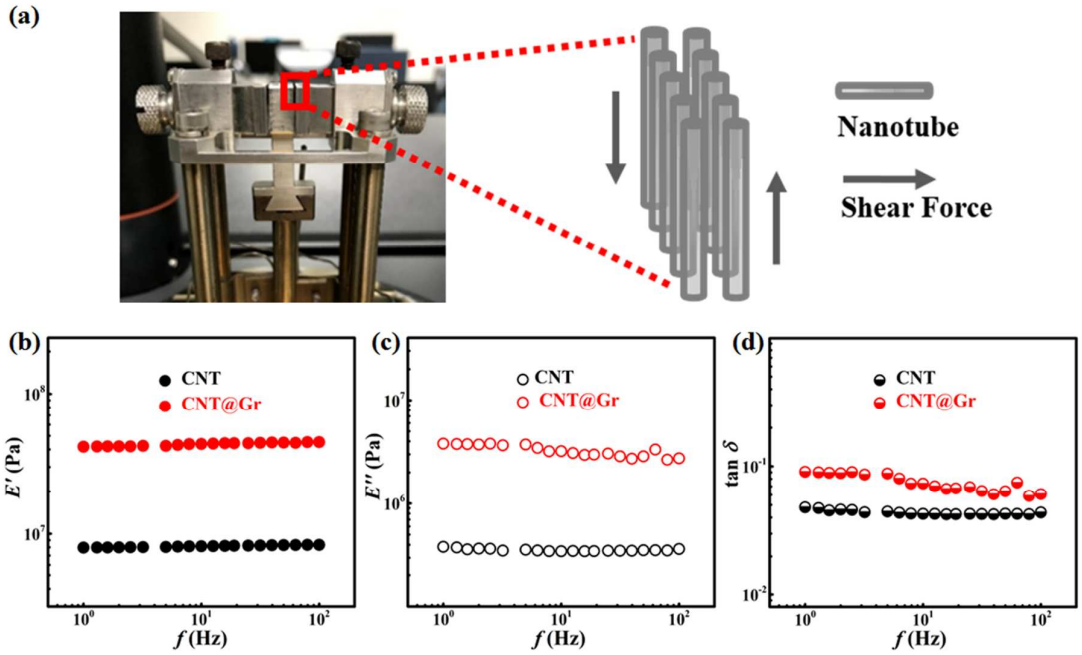

Figure S7 Dynamic shear tests of CNT and CNT@Gr arrays. (a) Shear sandwich clamp was used to measure the longitudinal shear viscoelastic properties of the NT arrays. (b) Storage modulus (*E'*), (c) loss modulus (*E''*) and (d) damping ratio (tan δ) of the CNT and CNT@Gr arrays as functions of applied frequency (*f*) (1−100 Hz, at ε = 2%).

Dynamic shear tests. Upon the applied shear loading of ε = 2% over the broad *f* range, the CNT@Gr arrays perform generally stable *E'* and *E''* of ~41.7 and ~3.8 MPa, respectively, which are ~5− and ~10−fold higher than those of their CNT counterpart (~8.0 and ~0.38 MPa, respectively). As a result, the CNT@Gr arrays shows ~2−fold increase in the tan δ (~0.1) as compared to the CNT arrays (~0.045). These substantial enhancements in the longitudinal shear viscoelastic properties of the CNT@Gr arrays indicate their reinforced inter-tube interactions because of the enlarged tube diameter and strengthened tube-tube contacts as compared to CNT arrays, which contribute to their enhanced compressive strength and viscoelasticity.

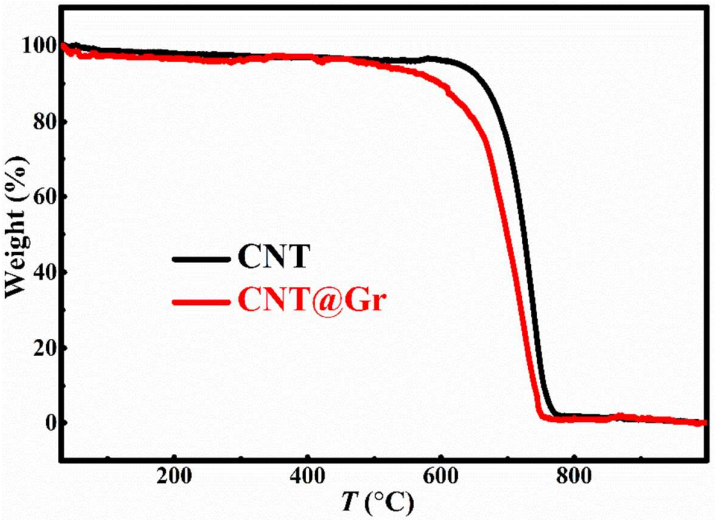

Figure S8 TGA analysis of CNT and CNT@Gr under a constant air flow of 50 mL min^{-1}. With the encapsulation of oxidation resistant graphene layers, the CNT@Gr generally retains the thermal stability of CNT in ambient air.

References

1. Fitzer, E.; Frohs, W.; Heine, M. Optimization of Stabilization and Carbonization Treatment of Pan Fibres and Structural Characterization of the Resulting Carbon Fibres. *Carbon* **1986**, *24*, 387−395.

2. Kim, K. H.; Oh, Y.; Islam, M. Graphene Coating Makes Carbon Nanotube Aerogels Superelastic and Resistant to Fatigue. *Nat. Nanotechnol.* **2012**, *7*, 562−566.

3. Brydson, R.; Zhili, Z.; Brown, A. In *Revisiting the Determination of Carbon sp^2/sp^3 Ratios via Analysis of the EELS Carbon K-Edge*, EMC 2008 14th European Microscopy Congress, Aachen, Germany, Sept 1–5, 2008; Luysberg, M., Tillmann, K., Weirich, T., Eds.; Springer, Berlin, Heidelberg, 2008.

4. Galvan, D.; Pei, Y.; De Hosson, J. T. M.; Cavaleiro, A. Determination of the sp^3 C Content of a-C Films Through EELS Analysis in the TEM. *Surf. Coat. Technol.* **2005**, *200*, 739−743.

5. Zhang, S.; Zeng, X.; Xie, H.; Hing, P. A Phenomenological Approach for the I_d/I_g Ratio and sp^3 Fraction of Magnetron Sputtered a-C Films. *Surf. Coat. Technol.* **2000**, *123*, 256−260.

6. You, B.; Wang, L.; Yao, L.; Yang, J. Three Dimensional N-Doped Graphene-CNT Networks for Supercapacitor. *Chem. Commun.* **2013**, *49*, 5016−5018.

7. Díaz, J.; Paolicelli, G.; Ferrer, S.; Comin, F. Separation of the sp3 and sp2 Components in the C1s Photoemission Spectra of Amorphous Carbon Films. *Phys. Rev. B* **1996**, *54*, 8064.

8. Bennett, M.; Ker, R. The Mechanical Properties of the Human Subcalcaneal Fat Pad in Compression. *J. Anat.* **1990**, *171*, 131.